14th European Signal Processing Conference (EUSIPCO 2006), Florence, Italy, September 4-8, 2006, copyright by EURASIP

FREQUENCY SELECTIVE DETECTION OF NQR SIGNALS IN THE PRESENCE OF MULTIPLE POLYMORPHIC FORMS

Samuel Somasundaram[†], *Andreas Jakobsson*[‡] *and John. A. S. Smith*[†]

[†] Depts. of Mechanical Engineering and Chemistry, King's College London, UK.
[‡] Dept. of Electrical Engineering, Karlstad University, Sweden.

ABSTRACT

Nuclear quadrupole resonance (NQR) is a radio frequency (RF) technique that detects compounds in the solid state and is able to distinguish between different polymorphic forms of certain compounds. For example, a typical sample of trinitrotoluene (TNT) will contain at least two polymorphic forms with rather different NQR properties. In this paper, we propose a frequency selective hybrid detector that exploits the presence of such polymorphic forms. The presented detector offers both improved probability of detection, as compared to recently proposed detectors, and allows for an estimation of the relative proportions of the multiple polymorphic forms.

1. INTRODUCTION

Nuclear quadrupole resonance (NQR) is a solid state, pulsed radio frequency (RF) technique that can be used to detect signals from quadrupolar nuclei, a requirement that is fulfilled by roughly 50% of the periodic table. Unlike NMR and MRI, NQR does not require a large static magnetic field to split the energy levels of the nucleus [1], making it attractive as a non-invasive technique, for instance, in the detection of hidden narcotics, such as cocaine and heroine, and explosives, e.g., for landmine detection [2]. Many chemical compounds form different crystalline structures known as polymorphic forms or polymorphs. Unambiguous detection and quantification of these forms is important in several applications. For instance, the varying intermolecular interactions among polymorphs can give rise to different pharmaceutical properties in medical drugs [3]. Another example is TNT, a common explosive in landmines, which exists in mainly two polymorphic forms, monoclinic and orthorhombic. Typically, it is of significant interest to either determine the relative quantity of the existing polymorphs, or to exploit the combined signals from all contained polymorphs to improve on the probability of detection (for a given false alarm), facilitating a faster and safer detection. Recently, we proposed various detectors that examine responses from a single polymorph [4–6]. Such detectors, which can only rely on resonant lines from one polymorph, will suffer if other polymorphs are also present. Herein, we present a hybrid detector which accounts for signals from multiple polymorphs and allows for estimates of the proportions of these polymorphs. The algorithm constructs a detection variable from a frequency selective data set, allowing for significant robustness in case of typically present residual RF interference (RFI). Evaluation of the algorithm using measured NQR signals indicate that the presented technique offers a significantly improved probability of accurate detection for samples containing more than one polymorphic form. For signals containing only one polymorphic form, the hybrid detector simplifies to the so-called Frequency selective Echo Train Approximate Maximum Likelihood (FETAML) detector introduced in [6].

This work was supported in part by the Defence, Science and Technology laboratories (DSTL), UK, and Carl Trygger's foundation, Sweden.

2. DATA MODEL

As described in [6], the mth NQR echo, produced by the pth polymorph, can be well modelled as

$$y_m^{(p)}(t) = \sum_{k=1}^{d^{(p)}} e^{-(t+m\mu)\eta_k^{(p)}(\tau)} \alpha_k^{(p)} e^{-\beta_k^{(p)}|t-t_{sp}|+i\omega_k^{(p)}(\tau)t}, \quad (1)$$

where $t = t_0, \ldots, t_{N-1}$ is the echo sampling time, not necessarily being consecutive instances, but typically starting at $t_0 \neq 0$ to allow for the dead time between an excitation pulse and the first measured sample (after the pulse)[1]. For simplicity, we will hereafter assume a uniform sampling starting at t_0, but note that the detectors may be generalised to also allow for non-uniform sampling. Furthermore, $m = 0, \ldots, M-1$ is the echo number; t_{sp}, often called the *tau* spacing, is the time between the centre of the refocusing pulse[2] and the echo centre; $\mu = 2t_{sp}$ is the echo spacing; $\alpha_k^{(p)}$ and $\beta_k^{(p)}$ denote, for the pth polymorph, the (complex) amplitude and sinusoidal damping constant of the kth NQR frequency, respectively. Furthermore, $\omega_k^{(p)}(\tau)$ and $\eta_k^{(p)}(\tau)$ are the frequency shifting and the echo train damping shifting functions of the kth NQR frequency component of the pth polymorph, respectively, both of which generally depend on the (unknown) temperature, τ, of the examined sample. An important point to note is that the number of damped sinusoids, $d^{(p)}$, as well as the frequency shifting function and the echo train damping shifting function for each spectral line, $\omega_k^{(p)}(\tau)$ and $\eta_k^{(p)}(\tau)$, may be assumed to be *known*, whereas $\alpha_k^{(p)}$ as well as the temperature of the examined sample, τ, are *unknown*. Furthermore, the damping constants, $\beta_k^{(p)}$, are essentially known for a given sample, but as variations may exist between samples, we will here allow for an uncertainty also in these constants, modelling $\beta_k^{(p)}$ as unknown. For NQR signals of many samples, such as for TNT, the frequency shifting function at likely temperatures of the sample can be well modelled as [2, 7]

$$\omega_k^{(p)}(\tau) = a_k^{(p)} - b_k^{(p)}\tau, \quad (2)$$

[1] Accounting for the dead time is equivalent to accounting for a large contribution to the first order phase correction in the NQR spectrum.

[2] The term refocusing pulse refers to the pulse, for example in a pulsed-spin locking (PSL) sequence, which refocuses the transverse magnetisation to produce an echo.

where $a_k^{(p)}$ and $b_k^{(p)}$, for $k = 1,\ldots,d^{(p)}$, are given constants. Often, the relative ratio between the signal amplitudes is accurately known for a given examined sample and experimental set-up. To exploit this knowledge, we will let $\alpha_k^{(p)} = \rho\kappa_k^{(p)}$, where ρ and $\kappa_k^{(p)}$ denote the common scaling constant due to the signal power and the a priori known relative (complex) scalings between the $d^{(p)}$ signal components, respectively. Herein, we are interested in examining samples possibly containing multiple polymorphic forms. As a result, we extend the data model in (1) to consist of the NQR response from P polymorphs, writing the observed data as

$$y_m(t) = \sum_{p=1}^{P} \gamma_p y_m^{(p)}(t) + w(t), \tag{3}$$

where γ_p denotes the proportion of the pth polymorph, and $w(t)$ is an additive *coloured* noise. A further discussion on the colour of the additive noise can be found in [4]. It should be stressed that the frequency shifting functions for different crystalline structures are, in general, different. We note, that (3) will be equally true for samples containing two or more different quadrupolar nuclei whose resonance frequencies happen to lie within the measured frequency range.

3. THE FHETAML DETECTOR

Let

$$\mathbf{y}_{NM} = \left[\begin{array}{cccc} \mathbf{y}_N^T(0) & \ldots & \mathbf{y}_N^T(M-1) \end{array}\right]^T = \Omega\mathbf{g}_\gamma + \mathbf{w}_{NM}, \tag{4}$$

where $\mathbf{y}_N(m) = [y_m(t_0),\ldots,y_m(t_{N-1})]^T$ is the mth echo of the echo train, $\mathbf{w}_{NM}$ is defined similar to $\mathbf{y}_{NM}$ except $\mathbf{w}_N(m) = [w(t_0+m\mu),\ldots,w(t_{N-1}+m\mu)]^T$, Ω is an NM-by-P matrix (where each column represents a different polymorph) defined by

$$\begin{aligned} \Omega &= \left[\begin{array}{cccc} \text{vec}[\Xi_1] & \ldots & \text{vec}[\Xi_P] \end{array}\right] && (5)\\ \Xi_p &= \mathbf{A}^{(p)}_{\tau,\beta^{(p)}} Q^{(p)} && (6)\\ \mathbf{g}_\gamma &= \left[\begin{array}{cccc} \rho\gamma_1 & \ldots & \rho\gamma_P \end{array}\right]^T, && (7) \end{aligned}$$

where the operation vec$[\mathbf{X}]$ stacks the columns of matrix $\mathbf{X}$ on top of each other, and for the pth polymorph

$$\begin{aligned} \mathbf{A}^{(p)}_{\tau,\beta^{(p)}} &= \mathbf{B}^{(p)}_\tau \odot \mathbf{S}_{\beta^{(p)}} && (8)\\ \mathbf{S}_{\beta^{(p)}} &= \left[\begin{array}{ccc} S^{(p)}_{1,t_0} & \cdots & S^{(p)}_{d^{(p)},t_0} \\ \vdots & \ddots & \vdots \\ S^{(p)}_{1,t_{N-1}} & \cdots & S^{(p)}_{d^{(p)},t_{N-1}} \end{array}\right] && (9)\\ S^{(p)}_{k,t} &= e^{-\beta_k^{(p)}|t-t_{sp}|} && (10)\\ \mathbf{B}^{(p)}_\tau &= \left[\begin{array}{ccc} \zeta^{t_0}_{p,1} & \cdots & \zeta^{t_0}_{p,d^{(p)}} \\ \vdots & \ddots & \vdots \\ \zeta^{t_{N-1}}_{p,1} & \cdots & \zeta^{t_{N-1}}_{p,d^{(p)}} \end{array}\right] && (11)\\ \zeta_{p,k} &= e^{i\omega_k^{(p)}(\tau)-\eta_k^{(p)}(\tau)} && (12)\\ Q^{(p)} &= \left[\begin{array}{cccc} \Psi_0^{(p)} & \ldots & \Psi_{M-1}^{(p)} \end{array}\right] && (13) \end{aligned}$$

$$\begin{aligned} \Psi^{(p)} &= \left[\begin{array}{cccc} \psi_1^{(p)} & \ldots & \psi_{d^{(p)}}^{(p)} \end{array}\right]^T && (14)\\ \psi_k^{(p)} &= \kappa_k^{(p)} e^{-\eta_k^{(p)}(\tau)m\mu} && (15) \end{aligned}$$

with $(\cdot)^T$ and $\odot$ denoting the transpose and Schur-Hadamard (elementwise) product, respectively. As is well known, the maximum likelihood estimator is found as (see, e.g., [8])

$$\hat{\theta} = \arg\min_\theta \| \ \mathbf{y}_{NM} - \Omega\mathbf{g}_\gamma \ \|^2_{\mathbf{R}_w}, \tag{16}$$

where $\|\mathbf{U}\|^2_{\mathbf{W}} = \mathbf{U}^*\mathbf{W}^{-1}\mathbf{U}$, and

$$\theta = \left[\begin{array}{ccccccc} \rho & \gamma & \tau & \beta^{(1)} & \ldots & \beta^{(P)} \end{array}\right]^T, \tag{17}$$

where $\gamma = [\gamma_1,\ldots,\gamma_P]$, and $\beta^{(p)} = [\beta_1^{(p)},\ldots,\beta_{d^{(p)}}^{(p)}]$. Further, $\mathbf{R}_w = E\{\mathbf{w}_{NM}\mathbf{w}_{NM}^*\}$ denotes the noise covariance matrix, where $E\{\cdot\}$ and $(\cdot)^*$ denote the expectation and the conjugate transpose, respectively. As $\mathbf{R}_w$ is typically unknown, one is normally forced to use an estimate of $\mathbf{R}_w$, say $\hat{\mathbf{R}}_w$, in (16). Such an estimate can be formed in various ways; herein, we propose using a low-order approximative noise model that is derived from real noise data [4]. We note that one may form a whitened version of the data using an inverse filtering operation. As filtering a (damped) sinusoidal signal through a n-tap linear filter will yield a scaled and phase shifted version of the signal, the resulting whitened signal, $\mathbf{z}_{\tilde{N}M}$, can be expressed as

$$\mathbf{z}_{\tilde{N}M} = \tilde{\Omega}\mathbf{g}_\gamma + \mathbf{e}_{\tilde{N}M}, \tag{18}$$

where the $\tilde{N}M \times 1$ vector $\mathbf{e}_{\tilde{N}M}$ is a zero-mean complex white Gaussian noise with variance σ_e^2, with $\tilde{N} = N - n$, and

$$\begin{aligned} \tilde{\Omega} &= \left[\begin{array}{cccc} \text{vec}\,[\tilde{\Xi}_1] & \ldots & \text{vec}\,[\tilde{\Xi}_P] \end{array}\right] && (19)\\ \tilde{\Xi}_p &= \tilde{\mathbf{A}}^{(p)}_{\tau,\beta^{(p)}} \tilde{Q}^{(p)}, && (20) \end{aligned}$$

where $\tilde{\mathbf{A}}^{(p)}_{\tau,\beta^{(p)}}$ is formed from the last $\tilde{N}$ rows of $\mathbf{A}^{(p)}_{\tau,\beta^{(p)}}$, and

$$\tilde{Q}^{(p)} = \left[\begin{array}{cccc} \tilde{\Psi}_0^{(p)} & \ldots & \tilde{\Psi}_{M-1}^{(p)} \end{array}\right], \tag{21}$$

where

$$\left[\tilde{\Psi}_m^{(p)}\right]_k = \tilde{\kappa}_k^{(p)} e^{-\eta_k^{(p)}(\tau)m\mu}, \tag{22}$$

with $[\cdot]_k$ denoting the kth index, and

$$\tilde{\kappa}_k^{(p)} = \begin{cases} \kappa_k^{(p)} C\left(\lambda_k^{(p)}\right) & \text{For initial } \lfloor t_{sp} - \tilde{t}_0 \rfloor \text{ rows} \\ \kappa_k^{(p)} C\left(\tilde{\lambda}_k^{(p)}\right) & \text{Otherwise} \end{cases} \tag{23}$$

where $\lfloor x \rfloor$ denotes the integer part of x, $\tilde{t}_0 = t_0 + n$, $\lambda_k^{(p)} = e^{i\omega_k^{(p)}(\tau)+\beta_k^{(p)}-\eta_k^{(p)}(\tau)}$ and $\tilde{\lambda}_k^{(p)} = e^{i\omega_k^{(p)}(\tau)-\beta_k^{(p)}-\eta_k^{(p)}(\tau)}$. Furthermore, $C(\lambda_k^{(p)})$ denotes the AR prewhitening filter, defined as

$$C(z) = \sum_{k=0}^{n} c_k z^{-k}, \tag{24}$$

with n denoting the order of the filter (see [4] for further details on this model and how to evaluate the AR coefficients).

We stress that due to the required n-tap prewhitening filter, $\mathbf{z}_{\tilde{N}M}$ will only contain $\tilde{N}M$ samples. Using (18), the minimisation in (16) can be written as

$$\min_{\theta} \left\| \ \mathbf{z}_{\tilde{N}M} - \tilde{\Omega}\mathbf{g}_{\gamma} \ \right\|_F^2, \tag{25}$$

where $\|\cdot\|_F$ denotes the Frobenius norm. Assuming the sample temperature lies in a known temperature range, we may, using (2), determine the range of frequencies each of the sinusoidal components may be present in. Hence, a frequency selective detector that only considers these frequencies can be derived. Consider the frequency regions formed by

$$\left\{ \frac{2\pi k_1}{\tilde{N}}, \frac{2\pi k_2}{\tilde{N}}, \ldots, \frac{2\pi k_L}{\tilde{N}} \right\}, \tag{26}$$

with $k_1, \ldots, k_L$ being L given, not necessarily consecutive, integers selected such that (26) only consists of the possible frequency grid points for each of the $(d^{(1)} + \ldots + d^{(P)})$ signal components[3]; each such region is given by the minimal and maximal frequency values for that component considering the *measured* temperature and the size of the expected temperature uncertainty region. Denoting the measured temperature $\hat{\tau}_s$, and the temperature uncertainty region Δ_{τ_s}, the minimal and maximal frequency values for each component can be determined using (2) with $\tau = \hat{\tau}_s - \Delta_{\tau_s}$ and $\tau = \hat{\tau}_s + \Delta_{\tau_s}$, respectively. It should be stressed that each echo should be Fourier transformed individually as each refocusing pulse will reinitialise the signal. The Fourier transformed (prewhitened) data vector for the mth echo and kth frequency bin can be expressed as

$$\begin{aligned} Z_k^m &= \mathbf{v}_k^* \left(\begin{bmatrix} \Gamma_1 & \ldots & \Gamma_P \end{bmatrix} \mathbf{g}_{\gamma} \right) + E_k^m & (27) \\ \Gamma_p &= \tilde{\mathbf{A}}^{(p)}_{\tau,\beta^{(p)}} \tilde{\Psi}_m^{(p)}, & (28) \end{aligned}$$

where $E_k^m = \mathbf{v}_k^* \mathbf{e}_{\tilde{N}}^m$ represents the kth frequency bin of the prewhitened noise sequence associated with the mth echo, $\mathbf{e}_{\tilde{N}}^m$, and

$$\mathbf{v}_k = \begin{bmatrix} 1 & w_k & \ldots & w_k^{\tilde{N}-1} \end{bmatrix}^T, \tag{29}$$

with $w_k = e^{i2\pi k/\tilde{N}}$. Thus, over the (possibly overlapping) frequency regions of interest, (27) can be expressed as

$$\mathbf{Z}_L^m = \mathbf{V}_L^* \left(\begin{bmatrix} \Gamma_1 & \ldots & \Gamma_P \end{bmatrix} \mathbf{g}_{\gamma} \right) + \mathbf{E}_L^m, \tag{30}$$

where

$$\begin{aligned} \mathbf{Z}_L^m &= \begin{bmatrix} Z_{k_1}^m & \ldots & Z_{k_L}^m \end{bmatrix}^T & (31) \\ \mathbf{V}_L &= \begin{bmatrix} \mathbf{v}_{k_1} & \ldots & \mathbf{v}_{k_L} \end{bmatrix}, & (32) \end{aligned}$$

and where $\mathbf{E}_L^m$ is defined similar to $\mathbf{Z}_L^m$. Using (30), the data model for the whole echo train can be expressed as,

$$\mathbf{Z}_{LM} = \begin{bmatrix} (\mathbf{Z}_L^0)^T & \ldots & (\mathbf{Z}_L^{M-1})^T \end{bmatrix}^T = \Sigma\mathbf{g}_{\gamma} + \mathbf{E}_{LM}, \tag{33}$$

where $\mathbf{E}_{LM}$ defined similar to $\mathbf{Z}_{LM}$, and

$$\Sigma = \begin{bmatrix} \mathrm{vec}\left\{\mathbf{V}_L^* \tilde{\Xi}_1\right\} & \ldots & \mathrm{vec}\left\{\mathbf{V}_L^* \tilde{\Xi}_P\right\} \end{bmatrix}. \tag{34}$$

[3] Excluding frequency grid points of known strong RFI sources.

Using (33), the minimization in (16) can be approximated as

$$\min_{\theta} \left\| \ \mathbf{Z}_{LM} - \Sigma\mathbf{g}_{\gamma} \ \right\|_F^2. \tag{35}$$

The unstructured least squares estimate of $\mathbf{g}_{\gamma}$ can be found as

$$\hat{\mathbf{g}}_{\gamma} = [\Sigma^*\Sigma]^{-1}\Sigma^*\mathbf{Z}_{LM} = \Sigma^{\dagger}\mathbf{Z}_{LM}, \tag{36}$$

where $(\cdot)^{\dagger}$ denotes the Moore-Penrose pseudoinverse[4]. It should be stressed that as the measured signal is complex, the unstructured estimate $\hat{\mathbf{g}}_{\gamma}$ is likely complex too, especially in the likely case where there are discrepancies between the model and the measured data. Bearing this in mind, we allow for a complex scaling, forming the estimate of γ_k as

$$\hat{\gamma}_k = \frac{\left|[\hat{\mathbf{g}}_{\gamma}]_k\right|}{\sum_{k=1}^{P} \left|[\hat{\mathbf{g}}_{\gamma}]_k\right|}. \tag{37}$$

where $[\hat{\mathbf{g}}_{\gamma}]_k$ denotes the kth element in $\hat{\mathbf{g}}_{\gamma}$. As an alternative, one might instead form a constraint *structured* estimate of $\mathbf{g}_{\gamma}$; however, in our experience, doing so offers no significant gain. Inserting $\bar{\mathbf{g}}_{\gamma} = \begin{bmatrix} \hat{\gamma}_1 & \ldots & \hat{\gamma}_P \end{bmatrix}^T$ into (35), the least squares estimate of ρ can be found as $\hat{\rho} = \tilde{\mathbf{q}}_{\breve{\theta}}^{\dagger}\mathbf{Z}_{LM}$, yielding

$$\max_{\breve{\theta}} \ \mathbf{Z}_{LM}^* \Pi_{\tilde{\mathbf{q}}_{\breve{\theta}}} \mathbf{Z}_{LM} \ , \tag{38}$$

where $\breve{\theta} = \begin{bmatrix} \tau & \beta^{(1)} & \ldots & \beta^{(P)} \end{bmatrix}^T$, and

$$\begin{aligned} \tilde{\mathbf{q}}_{\breve{\theta}} &= \Sigma\bar{\mathbf{g}}_{\gamma} & (39) \\ \Pi_{\tilde{\mathbf{q}}_{\breve{\theta}}} &= \tilde{\mathbf{q}}_{\breve{\theta}}\tilde{\mathbf{q}}_{\breve{\theta}}^{\dagger} & (40) \end{aligned}$$

We note that from a computational view, one should exploit the fact that the indices of $\mathbf{V}_L^*\Gamma_p = \mathbf{V}_L^*\tilde{\mathbf{A}}^{(p)}_{\tau,\beta^{(p)}}\tilde{\Psi}_m^{(p)}$ form geometric series; the gth index of $\mathbf{V}_L^*\Gamma_p$ can be written as

$$[\mathbf{V}_L^*\Gamma_p]_g = \sum_{l=1}^{d^{(p)}} G_l^{(p)} \left(\Omega_{1,l,g}^{(p)} + \Omega_{2,l,g}^{(p)} \right), \tag{41}$$

where

$$\begin{aligned} G_l^{(p)} &= \kappa_l^{(p)} e^{[i\omega_l^{(p)}(\tau) - \eta_l^{(p)}(\tau)]\tilde{t}_0 - \eta_l^{(p)}(\tau)m\mu} & (42) \\ \Omega_{1,l,g}^{(p)} &= C(\lambda_l^{(p)}) e^{\beta_l^{(p)}(\tilde{t}_0 - t_{sp})} \Upsilon_{\nu_{p,l,g}} & (43) \\ \Upsilon_{\nu_{p,l,g}} &= \frac{(1 - \nu_{p,l,g}^{\lfloor t_{sp} - \tilde{t}_0 \rfloor + 1})}{1 - \nu_{p,l,g}} & (44) \\ \Omega_{2,l,g}^{(p)} &= C(\tilde{\lambda}_l^{(p)}) e^{-\beta_l^{(p)}(\tilde{t}_0 - t_{sp})} \Upsilon_{u_{p,l,g}} & (45) \\ \Upsilon_{u_{p,l,g}} &= \frac{u_{p,l,g}^{\lfloor t_{sp} - \tilde{t}_0 \rfloor + 1} - u_{p,l,g}^{t_{N-1} - \tilde{t}_0 + 1}}{1 - u_{p,l,g}} & (46) \end{aligned}$$

[4] We have here assumed that the P polymorphs differ sufficiently to ensure the invertability of $[\Sigma^*\Sigma]$ in (36). To the best of our knowledge, this will be the case for all known substances, but we note that should the matrix be poorly conditioned, one can instead form a low-rank approximation of the inverse (see, e.g., [9]).

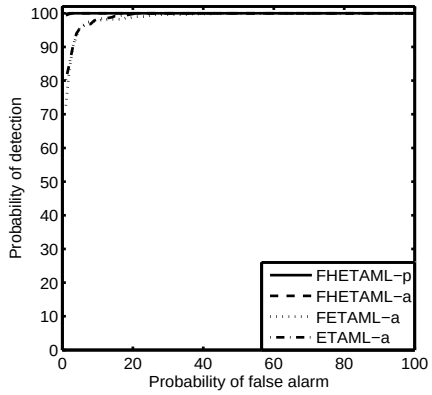

Figure 1: The ROC curves comparing the FHETAML-p, FHETAML-a, FETAML-a and ETAML-a detectors for partially shielded measured data.

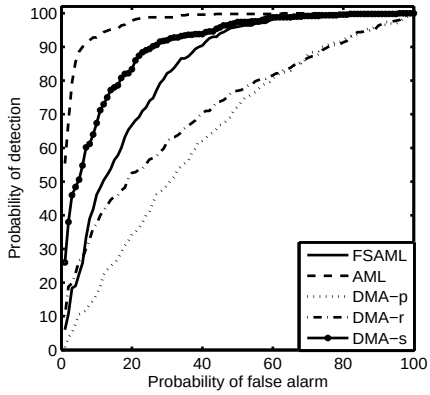

Figure 2: The ROC curves comparing the FSAML, AML, DMA-p, DMA-r and DMA-s detectors for partially shielded measured data.

$$u_{p,l,g} = e^{-i2\pi k_g/\tilde{N}+i\omega_l^{(p)}(\tau)-\eta_l^{(p)}(\tau)-\beta_l^{(p)}} \quad (47)$$

$$v_{p,l,g} = e^{-i2\pi k_g/\tilde{N}+i\omega_l^{(p)}(\tau)-\eta_l^{(p)}(\tau)+\beta_l^{(p)}}. \quad (48)$$

Using the $\breve{\theta}$ maximising (38), the test statistic is formed as

$$T(\mathbf{Z}_{LM}) = (LM-1)\frac{\mathbf{Z}_{LM}^* \Pi_{\tilde{\mathbf{a}}_{\breve{\theta}}} \mathbf{Z}_{LM}}{\mathbf{Z}_{LM}^* (\mathbf{I}-\Pi_{\tilde{\mathbf{a}}_{\breve{\theta}}}) \mathbf{Z}_{LM}}. \quad (49)$$

Using (49), the signal component is deemed present if and only if

$$T(\mathbf{Z}_{LM}) > \vartheta, \quad (50)$$

and otherwise not, where ϑ is a predetermined threshold value reflecting the acceptable probability of false alarm. To reflect that the resulting detector is a generalisation of the FETAML detector introduced in [6], we denote the here proposed detector the Frequency selective Hybrid ETAML (FHETAML) detector. To guarantee accurate estimates of all parameters, the full multidimensional minimisation described by (35) should be performed. Finding the multidimensional minimum using a grid search would require a quite dramatic complexity. As noted in [4–6], one can often, without significant loss in detector performance, use the approximations[5] $\beta_k^{(p)} \approx \beta_0^{(p)}$ and $\eta_k^{(p)} \approx \eta_0^{(p)}$, enabling the maximisation over $\breve{\theta}$ for a single polymorph to be approximated with the maximisation over $\breve{\theta}_{approx} = \left[\tau, \beta_0^{(p)}, \eta_0^{(p)}\right]$, being formed using three 1-D searches. Similarly, one can here form an approximation using (2P+1) 1–D searches over $\breve{\theta}_{approx} = \left[\tau, \beta_0^{(1)}, \ldots, \beta_0^{(P)}, \eta_0^{(1)}, \ldots, \eta_0^{(P)}\right]$. The (approximative) generalised likelihood ratio test can be formed using the obtained estimate $\breve{\theta}_{approx}$ in place of $\breve{\theta}$ in (49). This approximative detector is termed the FHETAML-a detector[6]. However, in our experience, the joint search space over the common (sinusoidal and echo train) damping constants will not decouple fully. As a result, one should rather form a common P–D search space over the P common sinusoidal damping constants, and similarly a P–D search space over the P common echo train constants. We term the resulting approximate detector, first forming a 1–D search over temperature, followed by a P–D search over the common sinusoidal damping constants and a P–D search over echo damping constants, respectively, the FHETAML-p detector.

4. NUMERICAL EXAMPLES

Herein, as an illustration of the applicability of NQR to polymorph detection, we will investigate the detection of TNT using the proposed detector[7]. TNT is a common explosive in landmines and currently poses a great challenge for the detection of landmines using NQR. Detection of TNT is complicated by the existence of at least two polymorphic forms, monoclinic and orthorhombic, with different NQR properties, e.g., different temperature shifting functions [10]. Landmines often contain a mixture of these two forms, the proportions of which can vary between landmines (and over time in a given landmine) as the metastable orthorhombic form may change slowly to the more stable (at room temperature) monoclinic phase. Herein, we will limit our attention to examine two of the polymorphic forms of TNT, i.e., $P = 2$, namely the monoclinic ($p = 1$) and the orthorhombic ($p = 2$) polymorphs. As detection is the problem of interest, the FHETAML-p and -a implementations were compared to the ETAML-a, FETAML-a, AML, FSAML, DMA-p, DMA-r and DMA-s detectors described in [4–6, 11]. The commonly used demodulation approach (DMA) measures the response of a single *a priori known* resonance frequency, with

[5] As shown in [6], one can in cases where the temperature shifting function of $\eta_k^{(p)}(\tau)$ is not fully known, instead treat $\eta_k^{(p)}(\tau)$ as a deterministic constant, using the approximation $\eta_k^{(p)}(\tau) \approx \eta_k^{(p)}$. In our experience, there is no significant loss by using this approximation and searching for $\eta_k^{(p)}$, as compared to exploiting the temperature shifting functions. As this approximation allows for not performing the full (rather time consuming) temperature shifting mapping, we will, when appropriate, hereafter use this approximation.

[6] In naming the FHETAML-a detector, we have followed the naming conventions used for naming the different ETAML/FETAML detectors introduced in [6].

[7] The authors are grateful to Dr. Jamie Barras and Dr. Mike Rowe at King's College London for their invaluable help in the NQR laboratory, to Ms Kate Long at DSTL for making the mixed TNT sample available, and to Dr. Kaspar Althoefer for his continuing support for the project.

DMA-p assuming perfect temperature knowledge. Furthermore, DMA-r assumes a more realistic temperature knowledge, using temperature values taken from a random variable, uniformly distributed over the interval $[\tau-5,\tau+5]$, where τ is the measured ambient temperature . Finally, DMA-s allows for a search in the relevant frequency region. All of the approximate maximum likelihood (AML) based techniques exploit the temperature dependencies of the sinusoidal components. The AML and FSAML detectors exploit the fine structure of the echo, hence, the AML, FSAML and DMA detectors are herein, applied to the summed echo train, formed by adding all the M consecutive echoes [4, 5, 11]. The ETAML and FETAML detectors exploit the temperature dependent spin-echo decay time, i.e. the fine structure of the echo train, hence, the FHETAML, ETAML and FETAML detectors are formed on the full echo train [6]. Furthermore, the AML, FSAML, ETAML, FETAML and DMA detectors were set-up assuming the sample was monoclinic TNT. The performance of the detectors is evaluated using measured NQR data, measured at King's College London. The measured data consisted of 1000 data files, 500 with TNT and 500 without, each containing four summed echo trains. The data was collected in a partially shielded environment, to allow for the typical practical case where some residual RFI remains. The sample, taken from an eastern European mine, weighed 500g and contained a mixture of monoclinic/orthorhombic TNT[8]. The temperature of the sample was not artificially controlled, to allow for the realistic case where temperature fluctuations would exist; however, the ambient air temperature was measured as 301K. The frequency shifting function constants for the $d^{(2)}=4$ orthorhombic lines are $a_1^{(2)}=891.021$, $a_2^{(2)}=874.876$, $a_3^{(2)}=891.613$, $a_4^{(2)}=872.054$ (all $a_k^{(p)}$ in kHz), $b_1^{(2)}=0.1454$, $b_2^{(2)}=0.0963$, $b_3^{(2)}=0.1692$ and $b_4^{(2)}=0.1184$ (all $b_k^{(p)}$ in kHzK^{-1}). The corresponding constants for monoclinic TNT can be found in [4, 6]. The a priori magnitude scalings, obtained from a pure monoclinic sample, for monoclinic TNT are $|\kappa_1^{(1)}|=0.3$, $|\kappa_2^{(1)}|=0.8$, $|\kappa_3^{(1)}|=1.0$ and $|\kappa_4^{(1)}|=0.65$. The a priori complex scalings for the orthorhombic lines, obtained from a pure monoclinic sample and predominantly orthorhombic sample, are $|\kappa_1^{(2)}|=0.3$, $|\kappa_2^{(2)}|=0.6$, $|\kappa_3^{(1)}|=1.0$ and $|\kappa_4^{(1)}|=0.1$. To account for temperature uncertainties, the AML-based detectors and the DMA-s detector use a search region over temperature of [290,310]K (in 100 steps). All the AML-based algorithms allow for uncertainties in the NQR sinusoidal damping parameters, and the ETAML, FETAML and FHETAML allow for uncertainties in the NQR echo damping parameters, by using the following search regions; the common sinusoidal damping parameters, $\beta_0^{(1)}$ and $\beta_0^{(2)}$, used searches of [0.001,0.1] in 100 steps; the common echo damping parameters, $\eta_0^{(1)}$ and $\eta_0^{(2)}$, used searches of [0.0001,0.0004] in 100 steps. It is stressed that these search spaces cover a large range of parameter values, and that in practice the range of these searches should be significantly more restricted given typical prior knowledge about the sample temperature, sinusoidal damping parameters and echo damping parameters. This will further improve the performance of all the AML based methods. We chose not to restrict our searches, in order to represent the worst case, where little is known about the NQR parameters. As detection is the problem of interest, we proceed to examine the receiver operator characteristic (ROC) curves for the detectors. Figures 1–2 show the ROC curves of the detectors, for the measured data set (described earlier). The figures clearly show the beneficial performance of the hybrid detectors over the other detectors. The FHETAML-p performs slightly better than FHETAML-a (although this is difficult to see from the printed figure), however, both perform significantly better than the non-hybrid detectors.

[8] Inspection of the spectrum for this sample, reveals that it is predominantly orthorhombic TNT.

REFERENCES

[1] A. N. Garroway, M. L. Buess, J. B. Miller, B. H. Suits, A. D. Hibbs, A. G. Barrall, R. Matthews, and L. J. Burnett, "Remote Sensing by Nuclear Quadrupole Resonance," *IEEE Trans. Geoscience and Remote Sensing*, vol. 39, no. 6, pp. 1108–1118, June 2001.

[2] R. M. Deas, I. A. Burch, and D. M. Port, "The Detection of RDX and TNT Mine like Targets by Nuclear Quadruple Resonance," in *Detection and Remediation Technologies for Mines and Minelike Targets, Proc. of SPIE*, vol. 4742, 2002, pp. 482–489.

[3] E. Balchin, D. J. Malcolme-Lawes, I. J. F. Poplett, M. D. Rowe, J. A. S. Smith, G. E. S. Pearce, and S. A. C. Wren, "Potential of Nuclear Quadrupole Resonance in Pharmaceutical Analysis," *Analytical Chemistry*, vol. 77, pp. 3925–3930, 2005.

[4] A. Jakobsson, M. Mossberg, M. Rowe, and J. Smith, "Exploiting Temperature Dependency in the Detection of NQR Signals," to appear in *IEEE Transactions on Signal Processing*.

[5] A. Jakobsson, M. Mossberg, M. Rowe, and J. A. S. Smith, "Frequency Selective Detection of Nuclear Quadrupole Resonance Signals," *IEEE Trans. Geoscience and Remote Sensing*, vol. 43, no. 11, pp. 2659–2665, November 2005.

[6] S. D. Somasundaram, A. Jakobsson, J. A. S. Smith, and K. Althoefer, "Exploiting Spin Echo Decay in the Detection of Nuclear Quadrupole Resonance Signals," submitted to *IEEE Trans. Geoscience and Remote Sensing.*

[7] J. A. S. Smith and M. D. Rowe, "NQR Testing Method and Apparatus," *Patent WO9945409*, 1999.

[8] P. Stoica and R. Moses, *Spectral Analysis of Signals*. Upper Saddle River, N.J.: Prentice Hall, 2005.

[9] G. H. Golub and C. F. V. Loan, *Matrix Computations*, 3rd ed. The John Hopkins University Press, 1996.

[10] R. M. Deas, M. J. Gaskell, K. Long, N. F. Peirson, M. D. Rowe, and J. A. S. Smith, "An NQR Study of the Crystalline Structure of TNT," in *Detection and Remediation Technologies for Mines and Minelike Targets, Proc. of SPIE*, vol. 5415, 2004, pp. 510–520.

[11] Y. Tan, S. L. Tantum, and L. M. Collins, "Cramer-Rao Lower Bound for Estimating Quadrupole Resonance Signals in Non-Gaussian Noise," *IEEE Signal Processing Letters*, vol. 11, no. 5, pp. 490–493, May 2004.